Title	Preparation of cytocompatible ITO neuroelectrodes with enhanced electrochemical characteristics using a facile anodic oxidation process
Authors	Vallejo-Giraldo, Catalina;Pampaloni, Niccolo Paolo;Pallipurath, Anuradha R.;Mokarian-Tabari, Parvaneh;O'Connell, John;Holmes, Justin D.;Trotier, Alexandre;Krukiewicz, Katarzyna;Orpella-Aceret, Gemma;Pugliese, Eugenia;Ballerini, Laura;Kilcoyne, Michelle;Dowd, Eilis;Quinlan, Leo R.;Pandit, Abhay;Kavanagh, Paul;Biggs, Manus Jonathan Paul
Publication date	2017-03-23
Original Citation	Vallejo-Giraldo, C., Pampaloni, N. P., Pallipurath, A. R., Mokarian-Tabari, P., O'Connell, J., Holmes, J. D., Trotier, A., Krukiewicz, K., Orpella-Aceret, G., Pugliese, E., Ballerini, L., Kilcoyne, M., Dowd, E., Quinlan, L. R., Pandit, A., Kavanagh, P. and Biggs, M. J. P. (2018) 'Preparation of cytocompatible ITO neuroelectrodes with enhanced electrochemical characteristics using a facile anodic oxidation process', Advanced Functional Materials, 28(12), 1605035 (18pp). doi: 10.1002/adfm.201605035
Type of publication	Article (peer-reviewed)
Link to publisher's version	https://onlinelibrary.wiley.com/doi/abs/10.1002/adfm.201605035 - 10.1002/adfm.201605035
Rights	© 2017, WILEY-VCH Verlag GmbH & Co. KGaA, Weinheim. All rights reserved. This is the peer reviewed version of the following article: Vallejo-Giraldo, C., Pampaloni, N. P., Pallipurath, A. R., Mokarian-Tabari, P., O'Connell, J., Holmes, J. D., Trotier, A., Krukiewicz, K., Orpella-Aceret, G., Pugliese, E., Ballerini, L., Kilcoyne, M., Dowd, E., Quinlan, L. R., Pandit, A., Kavanagh, P. and Biggs, M. J. P. (2018) 'Preparation of cytocompatible ITOneuroelectrodes with enhanced electrochemical characteristics using a facile anodic oxidation process', Advanced Functional Materials, 28(12), 1605035 (18pp). doi: 10.1002/adfm.201605035, which has been published in final form at https://doi.org/10.1002/adfm.201605035. This article may be used for non-commercial purposes in accordance with Wiley Terms and Conditions for Use of Self-Archived Versions.

ADVANCED FUNCTIONAL MATERIALS

Supporting Information

for *Adv. Funct. Mater.*, DOI: 10.1002/adfm.201605035

Preparation of Cytocompatible ITO Neuroelectrodes with Enhanced Electrochemical Characteristics Using a Facile Anodic Oxidation Process

Catalina Vallejo-Giraldo, Niccolò Paolo Pampaloni, Anuradha R. Pallipurath, Parvaneh Mokarian-Tabari, John O'Connell, Justin D. Holmes, Alexandre Trotier, Katarzyna Krukiewicz, Gemma Orpella-Aceret, Eugenia Pugliese, Laura Ballerini, Michelle Kilcoyne, Eilís Dowd, Leo R. Quinlan, Abhay Pandit, Paul Kavanagh, and Manus Jonathan Paul Biggs**

Supporting Information

Preparation of Cytocompatible ITO Neuroelectrodes with Enhanced Electrochemical Characteristics Using a Facile Anodic Oxidation Process.

Catalina Vallejo-Giraldo, Niccolò Paolo Pampaloni, Anuradha R. Pallipurath, John O'Connell, Justin D. Holmes, Parvaneh Mokarian-Tabari, Alexandre Trotier, Katarzyna Krukiewicz, Gemma Orpella-Aceret, Eugenia Pugliese, Laura Ballerini, Michelle Kilcoyne, Eilís Dowd, Leo R Quinlan, Abhay Pandit, Paul Kavanagh and Manus Jonathan Paul Biggs**

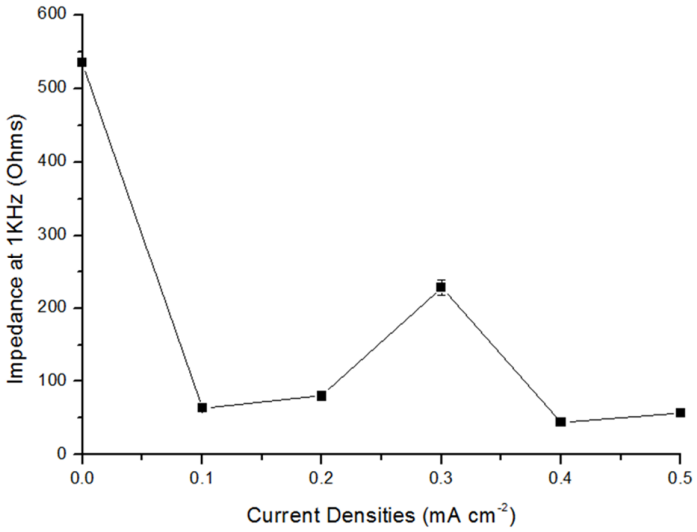

ITO Film	Impedance at 1 kHz (Ohms)
Pristine ITO	534.8 ± 2.6
0.1 mA cm^{-2}	63.3 ± 3.7
0.2 mA cm^{-2}	80.4 ± 6.2
0.3 mA cm^{-2}	227.7 ± 10.4
0.4 mA cm^{-2}	43.9 ± 3.6
0.5 mA cm^{-2}	56.8 ± 2.4

N=3

Figure S1. Optimization of current densities lower than 0.4 mA cm^{-2} through the impedance measurements at 1 kHz. Left, Plot of impedance magnitudes at 1 kHz of pristine ITO control and anodized films formed using current densities between 0.1 mA cm^{-2} and 0.5 mA cm^{-2}. Right, tabulated impedance magnitude values measured at 1 kHz for each of the films formed between 0.1 mA cm^{-2} and 0.5 mA cm^{-2} current densities. Overall, the anodized films formed at 0.4 mA cm^{-2} current density showed the lowest impedance magnitude at 1 kHz.

A)

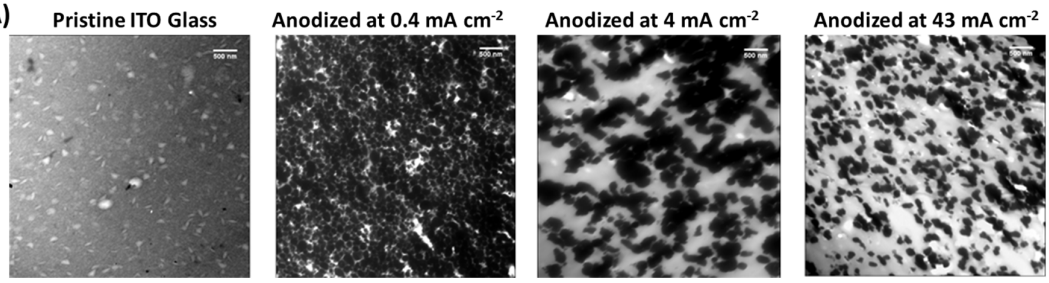

N=3

B)

ITO Film	Porosity [%]
Pristine ITO	3.1
Anodized at 0.4 mA cm^{-2}	15.3
Anodized at 4 mA cm^{-2}	54.4
Anodized at 43 mA cm^{-2}	42.8

Figure S2. Morphological characterization of the anodized ITO films. A) TEM images showing the structure and distribution of each of the anodized films and the pristine ITO glass control, scale bar = 500 nm B) Tabulated porosity percentages values for each of the experimental groups as an indication of the compactness of the particles forming each film.

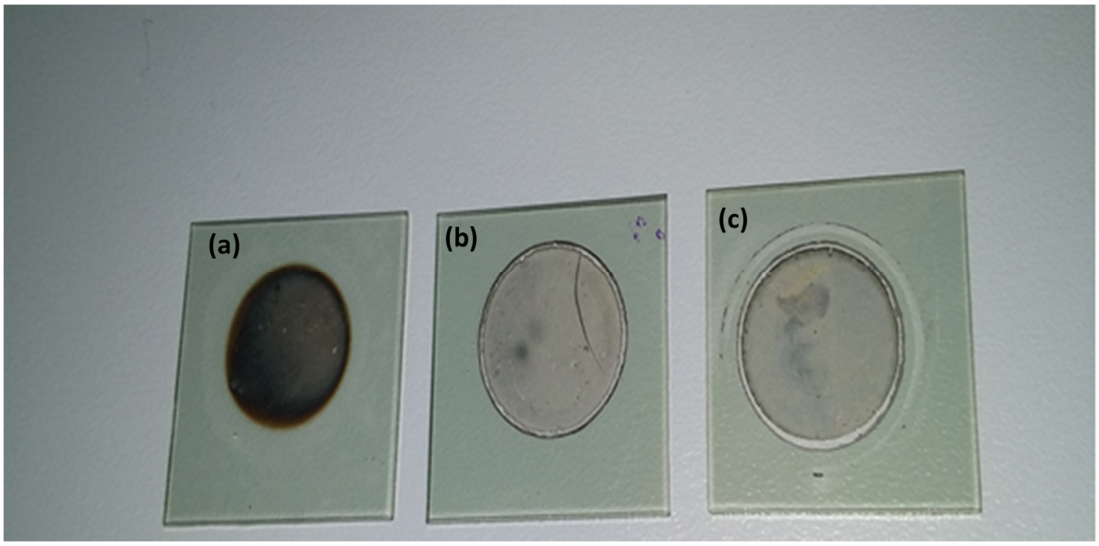

Figure S3. Visual color of the films which changed from a translucent blue-grey to an opaque dark grey . (a) Anodized ITO film 0.4 mA cm^{-2}, (b) Anodized ITO film at 4 mA cm^{-2} and anodized ITO film at 43 mA cm^{-2}.

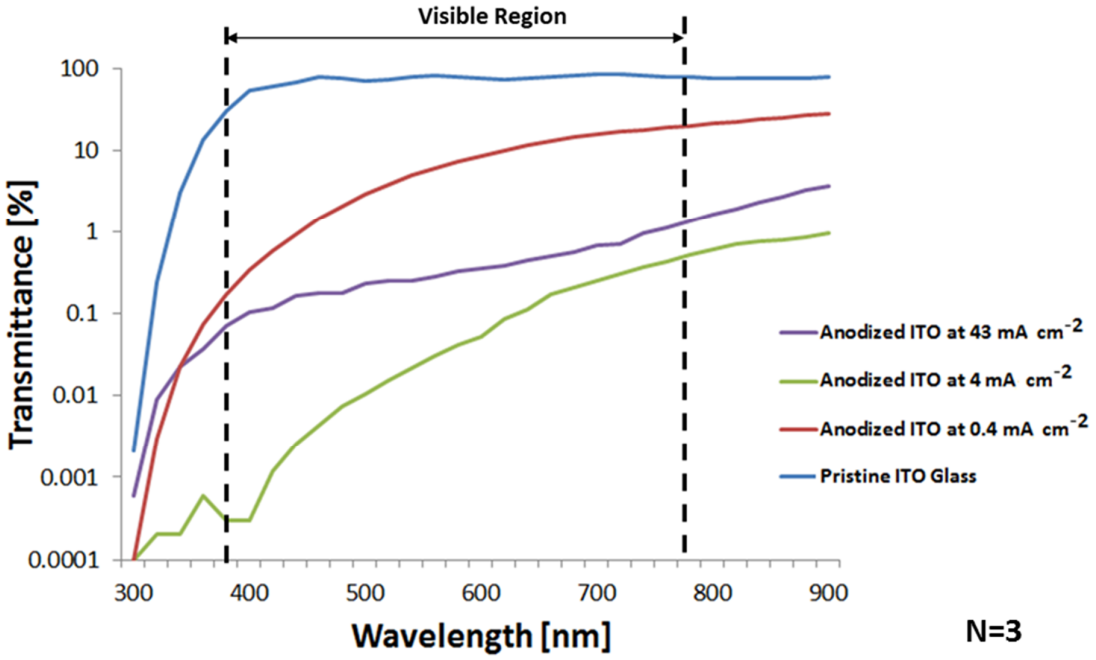

Figure S4. Optical transmission spectra of the pristine ITO coated glass and the anodic oxidized films formed at 0.4 mA cm^{-2}, 4 mA cm^{-2} and 43 mA cm^{-2} current densities.

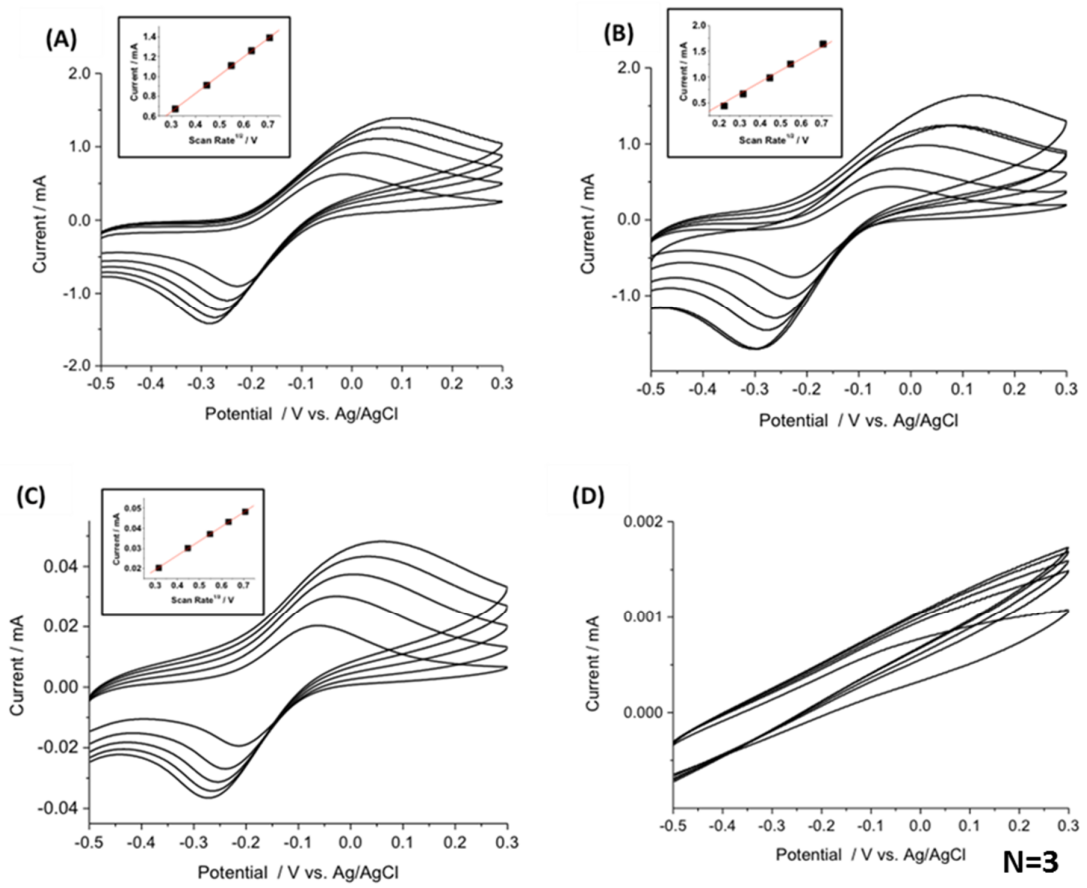

Figure S5. Cyclic voltammograms of (A) pristine ITO glass, and anodized ITO films formed at current densities of (B) 0.4 mA cm^{-2}, (C) 4 mA cm^{-2} and (D) 43 mA cm^{-2}, in 50 mM

phosphate buffer, pH 7.8, containing 2mM $[Ru(NH_3)_6]^{3+}$. Scan rates are 500, 400, 300, 200, and 100 mV s^{-1}, from outside inwards. (Inset: Plot of the square root of scan rate versus anodic peak (ip_a) currents).

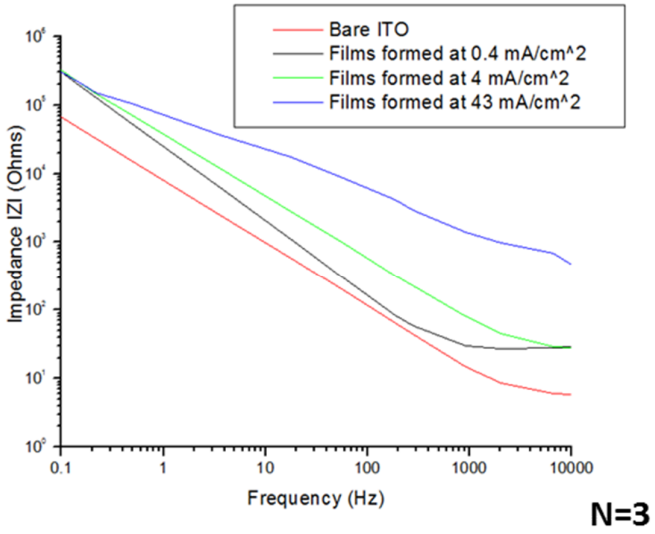

Figure S6. The presence of the polymer PSS in the solution is important for the anodization process. Films formed without the presence of PSS at 0.4 mA cm $^{-2,}$ 4 mA cm $^{-2}$ and 43 mA cm $^{-2}$ current densities revealed a linear increase in impedance compared to pristine ITO.

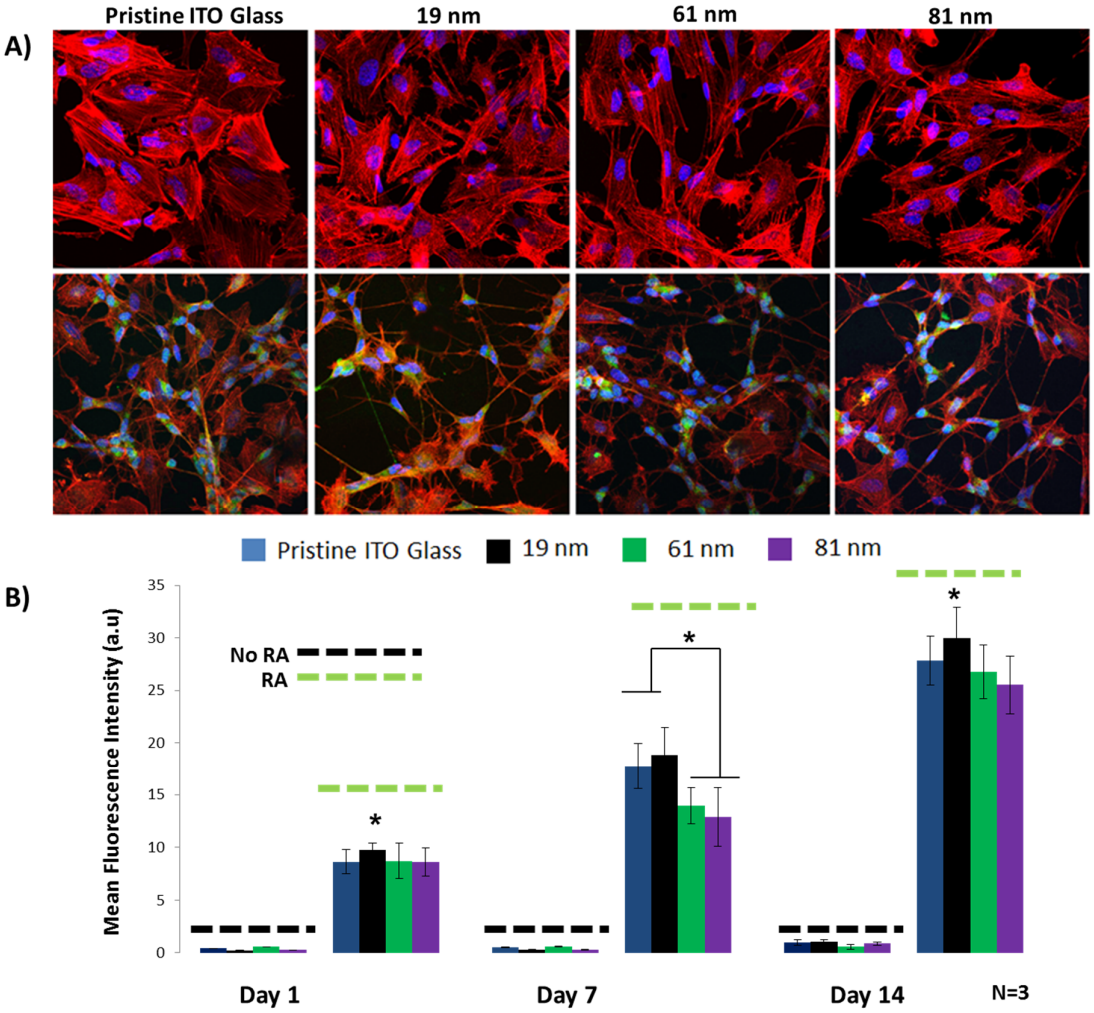

Figure S7. Expression of dopamine in SH-SY5Y neuroblastoma cell line. A) Fluorescent micrographs of immune-labelled cultures at day fourteen on pristine ITO glass and anodized ITO films with resulting roughness of 19 nm, 61 nm and 81nm. No RA supplementation (top) with RA supplementation films (bottom). Scale bar = 20um, objective 60x. Dopamine expression is visualized by anti- Anti-Tyrosine Hydroxylase (TH) in green, F-actin in red by rhodamine-conjugated phalloidin and in blue nuclei by Dapi. B) Mean fluorescence intensity quantification of dopamine expression using a threshold method. The TH dopamine marker was significantly upregulated following fourteen days of RA exposure, coupled with the induction of a neuronal phenotype. In addition, TH dopamine mean fluorescence intensity was significantly increased by day fourteen on the cells cultured on anodized films with the lowest roughness profile of 19 nm, which corresponds to the films formed at 0.4 mA cm^{-2} current density compared to control and the other experimental groups. Results are ± STD, ★ = $p < 0.05$.

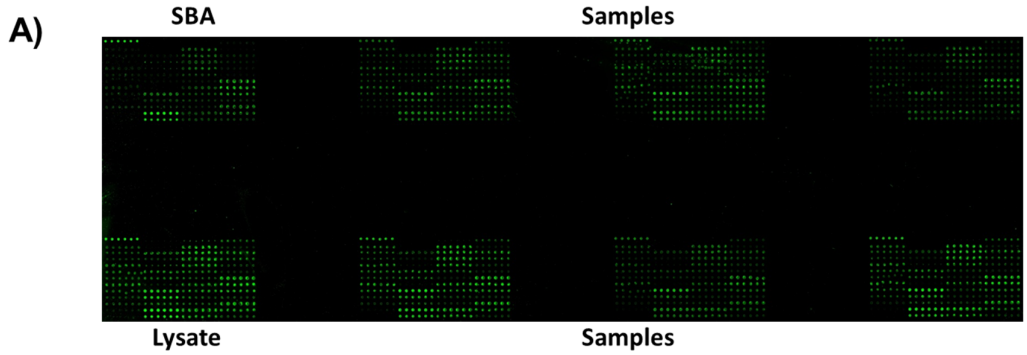

B)

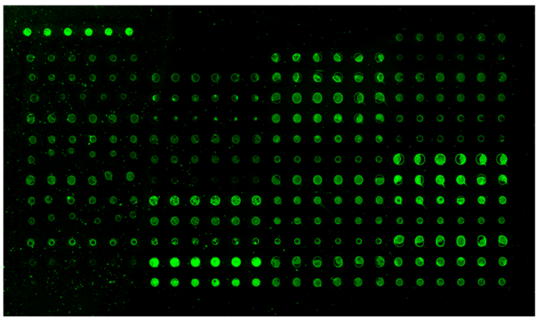

C)

GFAP_0.25	Iba1_0.25	PBS	PIEZO1_0.25
Nestin_1	Iba1_0.1	Anti-rat_0.5	PIEZO1_0.1
Nestin_0.5	Paxillin_1	Anti-sheep_0.5	PIEZO2_1
Nestin_0.25	Paxillin_0.5	VR1_1	PIEZO2_0.5
CD81_1	Paxillin_0.25	VR1_0.5	PIEZO2_0.25
CD81_0.5	C.Spectrin_0.5	VR1_0.25	PIEZO2_0.1
CD81_0.25	C.Spectrin_0.25	VR1_0.1	ANKTM1_1
OX42_1	C.Spectrin_0.1	L-type Ca2+_1	ANKTM1_0.5
OX42_0.5	Smad3_1	L-type Ca2+_0.5	ANKTM1_0.25
OX42_0.25	Smad3_0.5	L-type Ca2+_0.25	ANKTM1_0.1
Iba1_2.5	Smad3_0.25	L-type Ca2+_0.1	TREK1_1
Iba1_1	CS_0.1	PIEZO1_1	TREK1_0.5
Iba1_0.5	CS_0.05	PIEZO1_0.5	TREK1_0.25

Figure S8. Representative images from slides surface chemistries. A) Microarray experiments were carried out using three replicate slides. Alexa Fluor® 555 labelled healthy rat brain lysate (5 µg/mL) and soybean agglutinin (SBA) lectin (10 µg/mL) were used as internal controls and incubated in two separate subarrays on every slide to confirm retained antibody performance and printing, respectively. B). Individual representation image from a slide surface chemistry showing the subarrays. The subarrays were incubated and printed with each antibody following the order detailed in C) at a range of concentrations of 0.1 to 1 mg mL^{-1}.

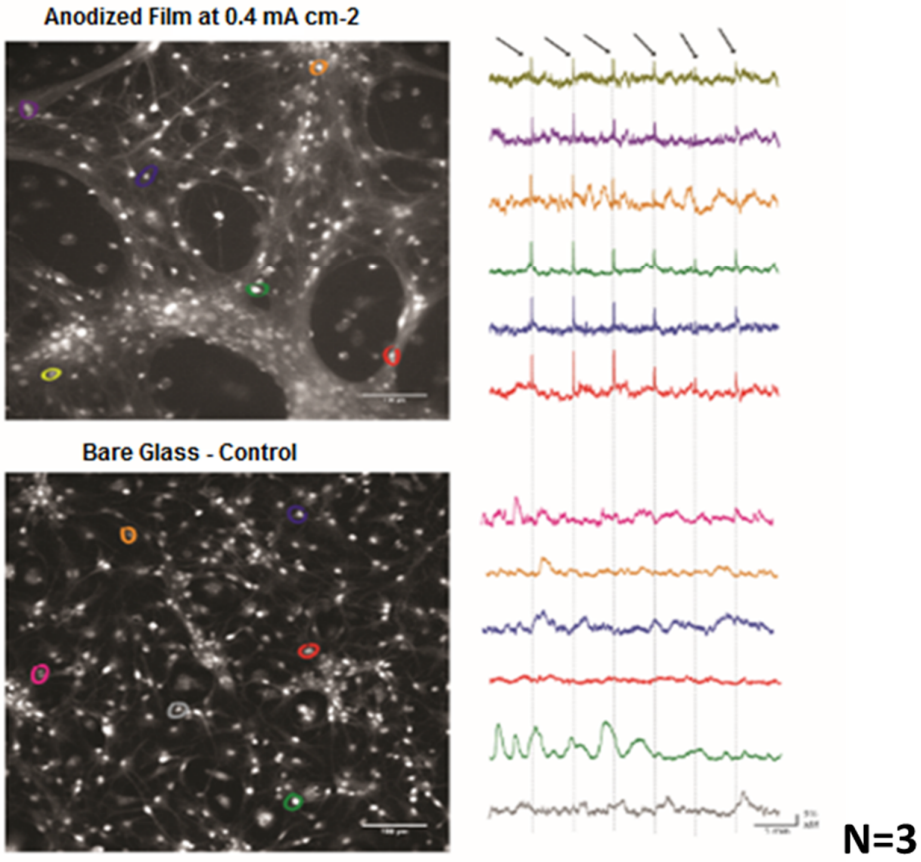

Figure S9. Calcium Imaging and Substrate Stimulation Left, snapshots of representative fields of neuronal cultures grown on 0.4 mA cm^{-2} (top) and control (bottom) and stained with the Oregon Green 488-BAPTA-1 AM. Six regions of interest (ROI) per images were selected (highlighted in different colors), each representing a single neuron, ROIs were selected at least 100 μm apart. Right, fluorescence tracings show the appearance of Ca^{2+} episodes, calcium events were measured from the relative ROI in the corresponding recording filed in both conditions (each cell is identified by the colour). In these experiments, voltage stimuli were delivered (every 60 seconds, arrows) via the substrate. Dashed lines highlight the corresponding evoked calcium response in both groups. Note that all selected cells displayed calcium transients in response to the stimulus in the 0.4 mA cm^{-2} condition, while the same stimulus did not elicit any responses in control cultures.

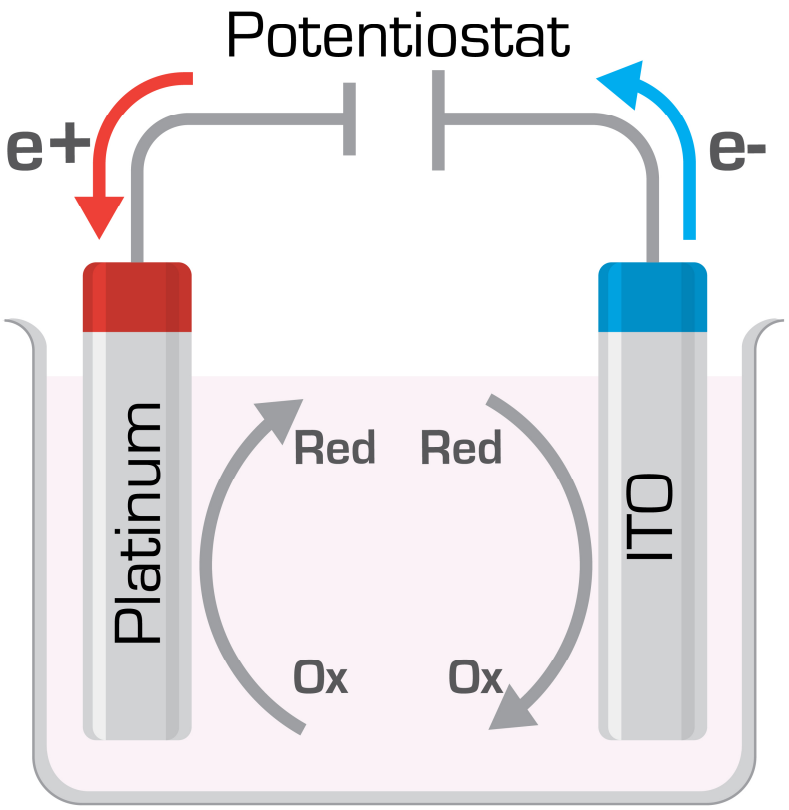

Figure S10. Schematic of the electrochemical set-up used for the anodization process

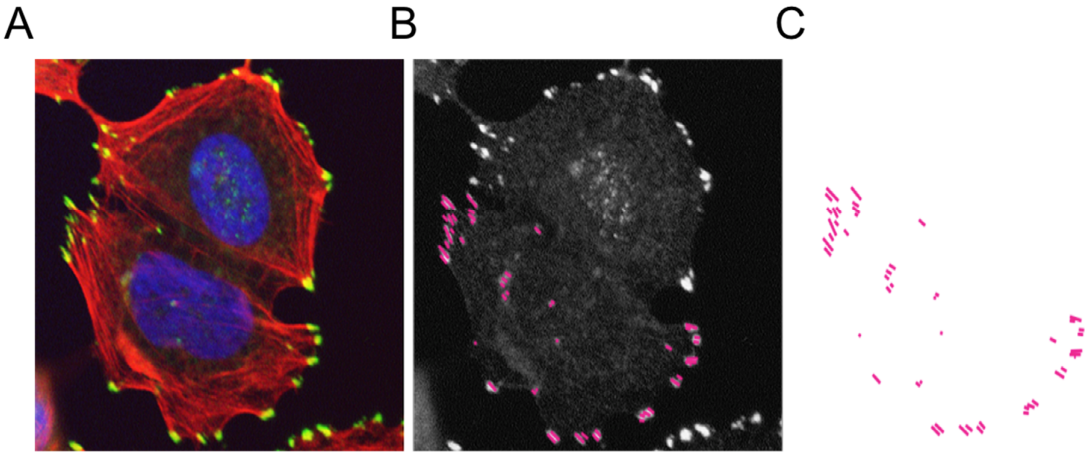

Figure S11. Methodology of FA analysis through ImageJ. Cells were labeled with anti-paxillin for FA imaging (Green), rhodamine conjugated phalloidin for actin imaging (red) and DAPI for nuclear imaging (blue) (A). The paxillin channel was subsequently isolated and individual FA sites were scored with a 4 pixel wide line (B). The individual lines were analysed by length and number (C) as described previously in [81].

Table S1. Summary of the all commercial antibodies used for the construction of gliosis antibody microarray

Order	Probe	Conc (mg/mL)	Information	Company	Ref
1	Anti-Glial Fibrillary Acidic Protein (GFAP)	0.25	Mouse anti-rat immunoglobulins, monoclonal	Sigma®	G3893
2	nestin (Rat-401)	1	Mouse anti-rat immunoglobulins, monoclonal	SantaCruz®	sc-33677
3	nestin (Rat-401)	0.5	Mouse anti-rat immunoglobulins, monoclonal	SantaCruz®	sc-33677
4	nestin (Rat-401)	0.25	Mouse anti-rat immunoglobulins, monoclonal	SantaCruz®	sc-33677
5	CD81 (H-121)	1	Rabbit anti-rat immunoglobulins, polyclonal	SantaCruz®	sc-9158
6	CD81 (H-121)	0.5	Rabbit anti-rat immunoglobulins, polyclonal	SantaCruz®	sc-9158
7	CD81 (H-121)	0.25	Rabbit anti-rat immunoglobulins, polyclonal	SantaCruz®	sc-9158
8	Integrin alphaM (OX42)	1	Mouse anti-rat immunoglobulins, monoclonal	SantaCruz®	sc-53086
9	Integrin alphaM (OX42)	0.5	Mouse anti-rat immunoglobulins, monoclonal	SantaCruz®	sc-53086
10	Integrin alphaM (OX42)	0.25	Mouse anti-rat immunoglobulins, monoclonal	SantaCruz®	sc-53086
11	Anti Iba1	2.5	Rabbit anti-rat immunoglobulins, polyclonal	WAKO®	019-19741
12	Anti Iba1	1	Rabbit anti-rat immunoglobulins, polyclonal	WAKO®	019-19741
13	Anti Iba1	0.5	Rabbit anti-rat immunoglobulins, polyclonal	WAKO®	019-19741
14	Anti Iba1	0.25	Rabbit anti-rat immunoglobulins, polyclonal	WAKO®	019-19741
15	Anti Iba1	0.1	Rabbit anti-rat immunoglobulins, polyclonal	WAKO®	019-19741
16	Paxillin antibody [Y113]	1	Rabbit anti-rat immunoglobulins, monoclonal	Abcam	ab32084
17	Paxillin antibody [Y113]	0.5	Rabbit anti-rat immunoglobulins, monoclonal	Abcam	ab32084
18	Paxillin antibody [Y113]	0.25	Rabbit anti-rat immunoglobulins, monoclonal	Abcam	ab32084
19	cleaved spectrin alpha II (h1186)	0.5	Rabbit anti-rat immunoglobulins, polyclonal	SantaCruz®	sc-23464
20	cleaved spectrin alpha II (h1186)	0.25	Rabbit anti-rat immunoglobulins, polyclonal	SantaCruz®	sc-23464
21	cleaved spectrin alpha II (h1186)	0.1	Rabbit anti-rat immunoglobulins, polyclonal	SantaCruz®	sc-23464
22	Anti-Smad3 antibody [EP568Y]	1	Rabbit anti-rat immunoglobulins, monoclonal	Abcam	ab40854
23	Anti-Smad3 antibody [EP568Y]	0.5	Rabbit anti-rat immunoglobulins, monoclonal	Abcam	ab40855
24	Anti-Smad3 antibody [EP568Y]	0.25	Rabbit anti-rat immunoglobulins, monoclonal	Abcam	ab40856
25	Anti-Chondroitin Sulfate antibody	0.1	Mouse anti-rat immunoglobulins, monoclonal	Sigma®	C8035
26	Anti-Chondroitin Sulfate antibody	0.05	Mouse anti-rat immunoglobulins, monoclonal	Sigma®	C8036
27	PBS		Phosphate buffered saline, pH 7.4		
28	Anti-rat_0.5	0.5	Rabbit anti-rat immunoglobulins, polyclonal	DAKO	
29	Anti-sheep_0.5	0.5	Rabbit anti-sheep immunoglobulins, polyclonal	DAKO	
30	VR1 (H-150)	1	Rabbit anti-human immunoglobulins, polyclonal	SantaCruz®	sc-20813
31	VR1 (H-150)	0.5	Rabbit anti-human immunoglobulins, polyclonal	SantaCruz®	sc-20813
32	VR1 (H-150)	0.25	Rabbit anti-human immunoglobulins, polyclonal	SantaCruz®	sc-20813
33	VR1 (H-150)	0.1	Rabbit anti-human immunoglobulins, polyclonal	SantaCruz®	sc-20813
34	Anticorps L-type Ca++ CP α1C (H-280)	1	Rabbit anti-human immunoglobulins, polyclonal	SantaCruz®	sc-25686
35	Anticorps L-type Ca++ CP α1C (H-280)	0.5	Rabbit anti-human immunoglobulins, polyclonal	SantaCruz®	sc-25686
36	Anticorps L-type Ca++ CP α1C (H-280)	0.25	Rabbit anti-human immunoglobulins, polyclonal	SantaCruz®	sc-25686
37	Anticorps L-type Ca++ CP α1C (H-280)	0.1	Rabbit anti-human immunoglobulins, polyclonal	SantaCruz®	sc-25686
38	PIEZO1 Antibody (N-15)	1	Goat anti-human immunoglobulins, monoclonal	SantaCruz®	sc-164319
39	PIEZO1 Antibody (N-15)	0.5	Goat anti-human immunoglobulins, monoclonal	SantaCruz®	sc-164319
40	PIEZO1 Antibody (N-15)	0.25	Goat anti-human immunoglobulins, monoclonal	SantaCruz®	sc-164319
41	PIEZO1 Antibody (N-15)	0.1	Goat anti-human immunoglobulins, monoclonal	SantaCruz®	sc-164319

Order	Probe	Conc (mg/mL)	Information	Company	Ref
42	PIEZO2 Antibody (G-20)	1	Rabbit anti-human immunoglobulins, polyclonal	SantaCruz®	sc-84763
43	PIEZO2 Antibody (G-20)	0.5	Rabbit anti-human immunoglobulins, polyclonal	SantaCruz®	sc-84763
44	PIEZO2 Antibody (G-20)	0.25	Rabbit anti-human immunoglobulins, polyclonal	SantaCruz®	sc-84763
45	PIEZO2 Antibody (G-20)	0.1	Rabbit anti-human immunoglobulins, polyclonal	SantaCruz®	sc-84763
46	ANKTM1 (C-19)	1	Goat anti-human immunoglobulins, polyclonal	SantaCruz®	sc-32353
47	ANKTM1 (C-19)	0.5	Goat anti-human immunoglobulins, polyclonal	SantaCruz®	sc-32353
48	ANKTM1 (C-19)	0.25	Goat anti-human immunoglobulins, polyclonal	SantaCruz®	sc-32353
49	ANKTM1 (C-19)	0.1	Goat anti-human immunoglobulins, polyclonal	SantaCruz®	sc-32353
50	TREK-1 Antibody (C-20)	1	Goat anti-human immunoglobulins, polyclonal	SantaCruz®	sc-11557
51	TREK-1 Antibody (C-20)	0.5	Goat anti-human immunoglobulins, polyclonal	SantaCruz®	sc-11557
52	TREK-1 Antibody (C-20)	0.25	Goat anti-human immunoglobulins, polyclonal	SantaCruz®	sc-11557